

7. ESTIMATE OF NON-PROMPT LOSSES

As well-confined fp's slow down in the Maxwellian background plasma, they can be lost to the wall by collisional pitch-angle scattering (PAS) into the loss region. For wall loading effects, it is important to estimate the size of the non-prompt losses relative to prompt bombardment. Assuming classical PAS (i.e., neglecting instability-induced losses during slowing down), it is found that the relative contribution of non-prompt losses is small. Still, the study of these losses is important as a "base case" comparison with instability-induced losses in future experiments, i.e., as a diagnostic [5,43,44] for studying the slowing down mechanism(s). Also, synergistic effects due to energy dependence and the angle-of-incidence of fp's reaching the wall may modify impurity evolution significantly.

7.1 Theory

Since fp energies considered here are much larger than the background plasma temperature ($E > 50$ keV), up-scattering due to velocity-space diffusion and losses by charge-exchange are neglected. In accord with previous work [18], small banana-width orbits and very untrapped particles are assumed. Under the above assumptions and in steady state, the resulting two-dimensional, bounce-averaged Fokker-Planck equation (derived by Rome et al.[18]) simplifies to:

$$\frac{1}{v^2} \frac{\partial}{\partial v} \left[(v^3 + v_c^3) g \right] + \frac{m_i v_c^3 Z_{\text{eff}}}{2m v^3} \frac{\partial}{\partial \zeta} \left[(1 - \zeta^2) \frac{\partial g}{\partial \zeta} \right] + s \tau_s = 0 \quad (7.1)$$

where $g = g(v, \zeta) =$ fp velocity-space distribution function,

$m =$ fp mass,

$Z_e =$ fp charge,

$v_c^3 = \frac{3\sqrt{\pi}}{4} \frac{m_e}{m_i} v_e^3 =$ critical velocity corresponding to equal slowing contributions by background ions and electrons.

$m_e, m_i =$ electron and background ion masses, respectively.

$v_e = \sqrt{2kT_e/m_e}$, for electron temperature, T_e ,

$Z_{\text{eff}} = \sum_j n_j Z_j^2 / n_e =$ effective charge of the background plasma,

$\zeta = \cos \chi$, evaluated when the drift orbit crosses the mid-plane ($\theta=0$)

$\tau_s = \frac{3\pi^{3/2} \epsilon_0^2 m m_e v_e^3}{n_e Z_e^2 q \ln \Lambda} =$ the Spitzer slowing down time for electronic charge q

$s =$ fp source rate.

These approximations are reasonable for counter-circulating fp's, because the trapping boundary usually coincides with the edge of the loss region; thus, the spatial deviation from a given flux surface doubles upon crossing this boundary [18]. Further, counter-circulating fp's, which scatter toward the loss region, have a slowing-down drift that is outward in r ; co-circulating fp's tend to drift inward [18,45]. This inward, slowing-down drift of co-circulating ions, together with the orbit topology [13] causes the

PAS across the χ_{\min} loss-region boundary to be zero. Thus, non-prompt fp losses occur predominantly across the χ_{\max} boundary, which is usually the x-type stagnation orbit. The small banana-width assumption (equivalent to neglecting variations in P_ϕ) tends to underestimate PAS for these counter-going particles. (Inclusion of the effect of large-banana widths requires a 3-D Fokker-Planck formulation: 2-D in velocity space (v, ζ) and 1-D in coordinate space. This is discussed in Chapters 8-11.)

The non-prompt loss fraction is estimated by integrating the second term in (7.1) over an element of velocity space. This is true, since the second term describes pitch-angle scattering which transports particles across the loss boundaries. The first term in Eqn. (7.1) describes slowing down in velocity magnitude only, i.e., motion parallel to the loss boundaries shown in Fig. 7.1. The result is

$$\frac{\delta F_{np}}{\delta E} = \frac{1}{S\delta E} \int_V 2\pi R r dr d\theta \int_{v+\Delta v}^v \pi dv \frac{m_i Z_{\text{eff}} v^3}{m v \tau_s} (1-\zeta^2) \left. \frac{\partial g}{\partial \zeta} \right|_{\zeta_1}, \quad (7.2)$$

where $\delta E = \frac{m}{2} [(v+\Delta v)^2 - v^2]$. The outer integral is evaluated over the plasma volume, V , and S is the total fusion source rate. The derivative of the distribution function in Eqn. 7.2, $\partial g/\partial \zeta$, is obtained by solving Eqn. 7.1 analytically with $g = 0$ at the boundary of the loss region. For this purpose, the loss region is approximated as shown in Fig. 7.1. As discussed above, only the χ_{\max}

FSL-78-6

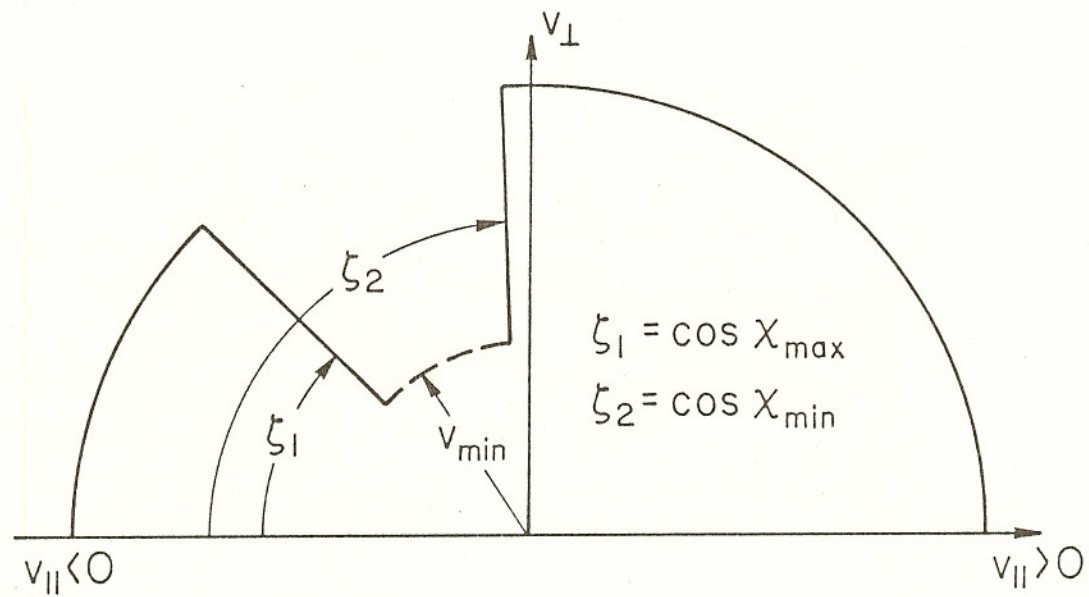


Figure 7.1 Velocity-space boundary conditions used in non-prompt loss calculation.

boundary is important, so the required constraint is $g(\zeta_1) = 0$,

where $\zeta_1 = \cos\chi_{\max}$. The result is:

$$\frac{\partial g}{\partial \zeta} \Big|_{\zeta_1} = \sum_{\nu} \frac{n_1 n_2 \langle \sigma v \rangle_{12} f_c \tau_s}{4\pi (v_0^3 + v_c^3)} \left(\frac{2\nu+1}{\nu(\nu+1)} \right) \left(\frac{\partial P_{\nu}}{\partial \zeta} / \frac{\partial P_{\nu}}{\partial v} \right)_{\zeta_1} \quad (7.3)$$

$$\times \left(\frac{v_0^3 + v_c^3}{v^3 + v_c^3} \right) \left(\frac{v}{v_c} \times \frac{v_0^3 + v_c^3}{v^3 + v_c^3} \right)^{\nu(\nu+1) m_i Z_{\text{eff}} / 6m},$$

where v_0 = initial fp velocity magnitude (corresponding to energy, E_0),

$P_{\nu}(\zeta)$ = Legendre function,

ν = spectrum of eigenvalues, obtained from $P_{\nu}(\zeta_1) = 0$,

$f_c = \frac{1}{2}(1 + \cos\chi_{\max})$ = differential fraction of fp's confined, having been born at (r, θ) with maximum loss angle, χ_{\max} .

Equation (7.2) can also be obtained by viewing PAS losses as non-re-entrant losses in velocity space. Using $g = 0$ at the loss-region boundary, the fp velocity-space current density, J_i , is [46-47]:

$$J_i = A_i g - D_{ij} \partial g / \partial v_j = -D_{ij} \partial g / \partial v_j, \quad (7.4)$$

where A_i is the kinematic coefficient. The net loss is then obtained by integrating J_i over an interval of velocity-space loss-region surface using the well-known form for the velocity-space diffusion tensor, D_{ij} , for an isotropic, Maxwellian plasma [46-47].

The method of calculation is as follows. First, the velocity-space loss region, $\chi_{\min} \leq \chi \leq \chi_{\max}$, is determined for a given fp

birth point in the plasma, (r_i, θ_i) . Second, for the x_{\max} orbit, $\zeta = \cos\chi|_{\theta=0}$, at $(r_{\min}, \theta=0) \leftrightarrow (x_{\min}, z=0)$, is obtained via a numerical, step-wise search. If the drift orbit intersects the mid-plane for $x_{\min} \leq 0$, the loss contributions due to this orbit are neglected for two reasons: 1) such orbits are a small class of the total (less than a few percent), and 2) orbits that form the x_{\max} boundary and have $x_{\min} < 0$ will have slowing-down drifts that are *inward* in r . The latter effect causes PAS across the x_{\max} loss boundary to be negligible, as in the case of co-circulating particles. Third, the derivative $\partial g / \partial \zeta$, is evaluated at $\zeta = \zeta_1$, using Eqn. (7.3). The Legendre functions of non-integer order, $P_\nu(\zeta)$, are determined using routines from the CERN Program Library [48]. The derivative, $\partial P_\nu / \partial \zeta$, is evaluated using [49]:

$$\frac{\partial P_\nu}{\partial \zeta} = \frac{\nu(P_{\nu-1} - \zeta P_\nu)}{1-\zeta^2} = \frac{\nu P_{\nu-1}(\zeta)}{1-\zeta^2},$$

since $P_\nu(\zeta) = 0$. While $\partial P / \partial \nu$ can be evaluated analytically [50], central differences are computationally faster:

$$\frac{\partial P_\nu}{\partial \nu} = \frac{P_{\nu+\Delta\nu} - P_{\nu-\Delta\nu}}{2\Delta\nu},$$

for $\Delta\nu = 5 \times 10^{-6}$. Finally, the integral in eqn. (7.3) is evaluated over the plasma volume.

7.2 Results

Typical results for the non-prompt alpha loss-fraction-per-keV in PLT and TFTR-1, are shown in Figs. 7.2-7.3. Since the drift orbit physics is the same here as for the prompt flux (depending on the direction of the toroidal B-field), the non-prompt losses occur either to the upper-half or to the lower-half surface of the device. The corresponding flux-per-keV, averaged over the upper-(lower-) half surface, is shown, as a companion ordinate, in these Figures.

Also shown in Figs. 7.2-7.3 are the cumulative particle loss fraction, ν_p , defined as:

$$\nu_p = \int_{E_0}^E \frac{\delta F_{np}}{\delta E} dE, \quad (7.5)$$

and the cumulative energy loss fraction, ν_E , given as:

$$\nu_E = \int_{E_0}^E \left(\frac{E}{E_0} \right) \frac{\delta F_{np}}{\delta E} dE. \quad (7.6)$$

As expected, both the ν_p and ν_E rise monotonically with decreasing alpha energy. The fastest change occurs close to the birth energy, indicating that MeV losses are dominant. This is discussed further below.

In PLT (Fig. 7.2), the loss-fraction-per-keV falls abruptly as the fp energy decreases below the birth energy, rises slowly to a

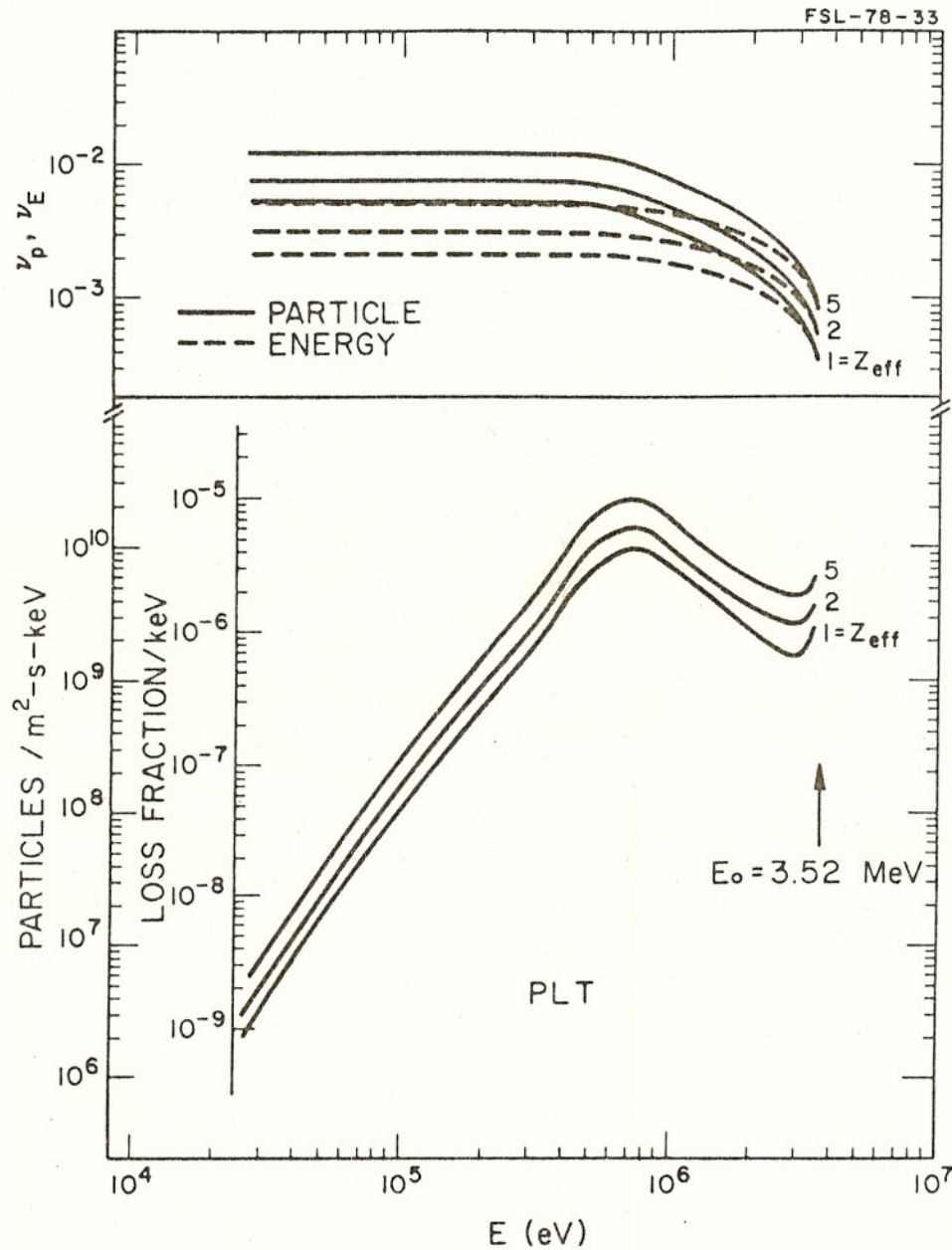


Figure 7.2 The lower figure shows the non-prompt alpha loss fraction per keV and average flux per keV versus particle energy in PLT. The upper figure shows ν_p and ν_E (cumulative particle- and energy-loss fractions, respectively) versus alpha energy in PLT.

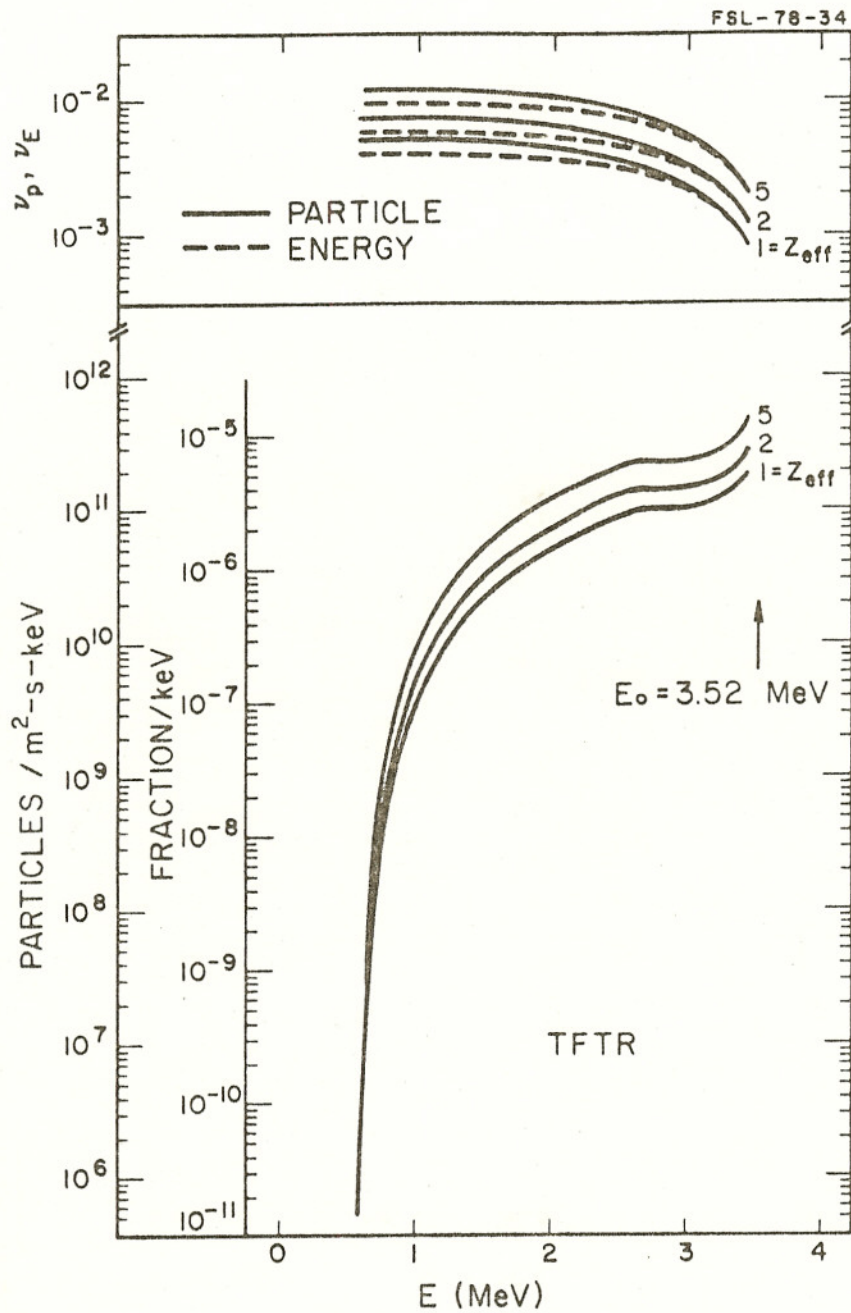


Figure 7.3 The lower figure shows the non-prompt alpha loss fraction per keV and average flux per keV versus particle energy in TFTR-I. The upper figure shows ν_p and ν_E (cumulative particle- and energy-loss fractions, respectively) versus alpha energy in TFTR-I.

maximum at $v \sim 2.7 v_c$, and then decreases monotonically. The abrupt drop in $\delta F_{np}/\delta E$, for $E < E_0$ is expected, due to particles in orbits very near the prompt-loss boundaries entering the loss region. The maximum at $v \sim 2.7 v_c$ occurs because PAS increases more rapidly than the loss region is decreasing. Below 700 keV, the decreasing loss region dominates PAS, yielding a monotonic drop in the losses. In larger machines like TFTR (Fig. 7.3), the loss region is completely dominant over PAS, giving a monotonic decrease in $\delta F_{np}/\delta E$ with decreasing fp energy. The results for ORNL-EPR and UWMAK-I are very similar to Fig. 7.3, and therefore are not shown.

The dependence of non-prompt losses on Z_{eff} can be gauged as follows. The asymptotic values of the v_p and v_E (i.e., as the fp speed approaching the minimum value at which escape can occur), are defined to be v_p^* and v_E^* respectively. The average energy, \bar{E} , of the non-prompt losses is obtained by combining (7.5) and (7.6).

$$\bar{E} = E_0 (v_E^*/v_p^*) . \quad (7.7)$$

Both v_p^* and v_E^* rise monotonically as Z_{eff} increases (see Fig. 7.4) with $v_p^* \leq 0.1 \times F_\ell \times \sqrt{Z_{eff}}$. The value of \bar{E} is constant with respect to Z_{eff} , indicating that increasing Z_{eff} yields a uniform rise in PAS for all velocities. In all cases, \bar{E} is greater than 1.4 MeV; for TFTR, ORNL-EPR, and UWMAK-I, \bar{E} is above 2.6 MeV. These large average energies indicate that most non-prompt losses occur near the birth energy (i.e. the loss region shrinks rapidly with decreasing speed).

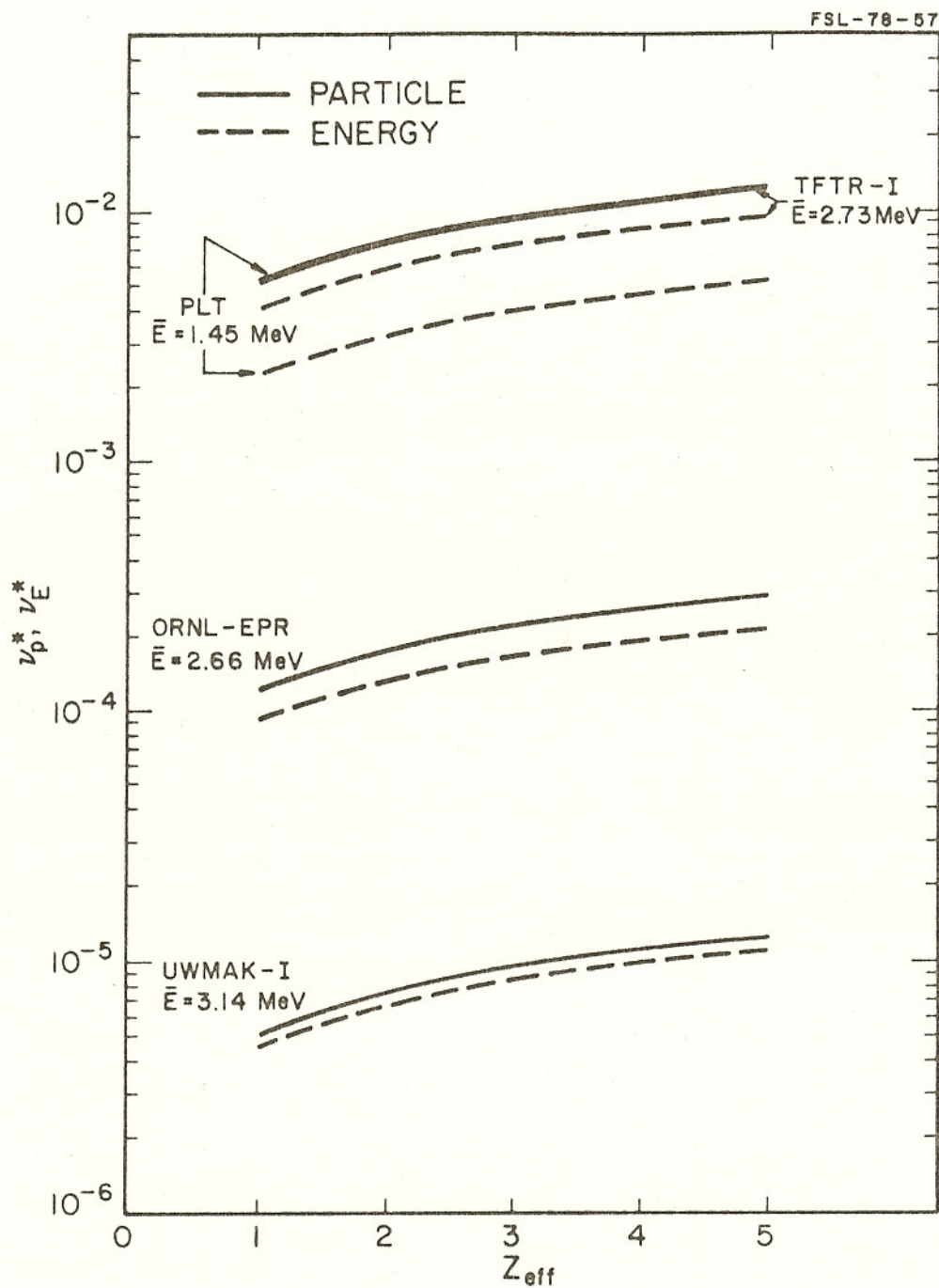


Figure 7.4 Asymptotic values of the cumulative particle- and energy-loss fractions (ν_p^* and ν_E^* , respectively) versus Z_{eff} for various tokamaks.

7.3 Comparison to Ohnishi's Work

Recently, Ohnishi et al., have also modeled alpha losses during slowing-down and pitch-angle-scattering [35] using a Monte Carlo method. They determine losses in JEPR (see Table 5.1) for a constant current density and temperature, with

$$n_i = 10^{20} [1 - 0.8(r/a)^2] (\text{m}^{-3}).$$

A comparison of the present results with their work [c.f. Fig. 9 of Ref. 35] is given in Table 7.1. The accuracy of our model was estimated by calculating non-prompt losses for extreme cases of

Table 7.1: Non-Prompt Alpha Loss Fraction

<Z>	Loss Fraction, %		Ratio (Ref. 35/Present)
	Ref. 35	Present Work	
1	1.41	0.56	2.5
2	2.06	0.81	2.5
3	2.67	1.00	2.7
4	3.43	1.16	3.0
5	4.14	1.31	3.2

slowing down on constant r -values at r_{max} and r_i [51]; the variation among these cases is less than a factor of 2 (see Appendix D).

Ref. 35 includes the effects of slowing-down drifts and large banana-width orbits, while our estimate excludes these effects. Consequently,

the factor of 2 difference between our results and Ref. 35 is not surprising. However, slowing-down drifts and large banana-width effects are independent of Z_{eff} [116]. Thus, it is puzzling that both the present work and Ref. 19 find non-prompt losses proportional to $\sqrt{Z_{\text{eff}}}$, while Ohnishi et al. find that these losses increase linearly in Z_{eff} . This difference is unresolved to date [115].

As discussed above, non-prompt losses are one-tenth of the prompt losses, and thus the former are unimportant consideration in the evaluation of alpha heating, even for large Z_{eff} . In contrast, Ohnishi et al. [35] conclude that non-prompt losses significantly reduce alpha heating. This is because they assumed constant current-density and particle-density. When more realistic parabolic J- and n-profiles are used, the losses from the EPR-size device considered by Ref. 35 are comparable to losses in ORNL-EPR.